Design and Characterization of a Flexible Self-Inflating Mechanical Structure

Soroush Kamrava
Department of Mechanical Engineering,
Northeastern University,
Boston, MA 02115
e-mail: kamrava.s@husky.neu.edu

Milad Tatari
Department of Mechanical Engineering,
Northeastern University,
Boston, MA 02115
e-mail: tatari.m@husky.neu.edu

Yustianto Tjiptowidjojo
Lecturer
Department of Mechanical Engineering,
Northeastern University,
Boston, MA 02115
e-mail: y.tjiptowidjojo@northeastern.edu

Hamid Nayeb-Hashemi
Professor
Department of Mechanical Engineering,
Northeastern University,
Boston, MA 02115
e-mail: hamid@coe.neu.edu

Inflatable structures are commonly used in a variety of engineering applications such as robotics, space structures, medical devices, and automotive safety devices. However, inflation in these systems often requires a non-flexible external pressurized fluid source. Integration of the pressurized fluid source and the flexible construct sacrifices some of the main advantages of the soft structures such as overall flexibility of the system, weight, and cost of fabrication. In this paper, we introduce a novel design for self-inflating structure with embedded pressurizing module. The design is based on integrating a flexible dome with a cylinder. The pressure inside the cylinder is controlled by subjecting dome to a cyclic compression, causing air exchange between the dome and the cylinder. The performance of this design is fully validated through finite element simulations using fluid structure interactions as well as experimental investigations. The results show that a higher pressure is achieved by having smaller dome height. In addition to controlling internal pressure of the cylinder, the design can be used to control the stiffness of the flexible structure such as soft robotics through pressurization. An application of this conceptual device such as pressurizing a tire is presented. This device is integrated within a tire and tire rotation as well as load on the tire have been shown to pressurize the tire. The final pressure and time to achieve maximum pressure depend on the load to the axel of the tire and tire rotational speed, respectively.
[DOI: 10.1115/1.4054953]

Keywords: 3D printing, additive manufacturing, analysis and design of components, devices, and systems, conceptual design

1 Introduction

Soft and reconfigurable structures are widely used in space structures [1–3], smart systems [4,5], and artistic applications [6,7] because of their tunable physical properties such as shape, color, surface morphology, and stiffness. These property variations are usually obtained through the alteration of the form, size, and strain state of the construct. Different techniques such as origami-inspired structural design [8,9] have been used to create such systems with tunable properties; however, inflation of a soft structure is a superior technique in terms of versatility, ease of integration with other soft systems, and cost of fabrication [1,10,11]. In terrestrial device applications, inflatable soft structures offer a wide range of shapes and properties for different purposes such as soft robotics [12–14] and wearable devices [15,16]. In the past, several inflatable structures have been developed to perform various engineering tasks. Rafsanjani et al. introduced a biomimetic crawling soft robot, where the inflation of a rubbery core structure changes frictional properties of the robot exterior surfaces and enables the robot to crawl forward [17]. In addition, Konishi and Kosawa developed an inflation-driven micro-actuator using a conversion mechanism to create high-output bending motion [18]. In another example, Gorissen et al. presented a spherical structure capable of harvesting low inflation rates to activate a snap-through instability-driven motion. This sudden release of energy can be used to make the structure jump [19]. These novel engineered systems operate with an external source of pressurized fluid, which is usually made from non-flexible and bulky stand-alone components. Integrating a rigid fluid pump with a soft structure may sacrifice the overall flexibility of the system and mitigate some of the main advantages of the soft structures. Our thorough literature survey did not result in any papers addressing design of flexible pumps and its incorporation in an integrated system to control stiffness of device. Our novel design allows such an integrated device which can be incorporated into soft robotic applications as well as other devices. There has been a lot of research in developing pumps in biomechanics applications. Cacucciolo et al. [20] designed a class of soft-matter bidirectional pumps based on charge-injection electrohydrodynamics. They showed that these solid-state pumps are flexible, stretchable, modular, scalable, quiet, and rapid. Furthermore, they integrated the designed pump into a glove and demonstrated wearable active thermal management. Sinn et al. [21] introduced an adaptive structure called the self-inflating adaptive membrane. They showed in a single structure that smart components can be incorporated by changing its shapes and flexibility to different mission requirements. The idea behind this adaptive design is taken from nature's heliotropism principle. It is shown that through this bio-inspired concept, a high ratio of adaptability of the membrane can be obtained. Diteesawat et al. [22] introduced the electro-pneumatic pump, a flexible, high-performance pneumatic pump driven by dielectrophoretic liquid zipping actuation that overcomes the limitations of conventional electromagnetic pneumatic power sources, generating higher air flowrate and consuming less power. Yamaguchi et al. [23] developed a soft pneumatic balloon operated by a soft pump which applies the appropriate pressure over a tactile sensor onto the radial artery of the wrist to detect detailed heart pulse waves (P1 and P2). Stergiopulos et al. [24] designed and manufactured a monolithic high-pressure diaphragm pump made entirely of soft elastomer material and driven by a combustion chamber incorporated within the soft pump structure. The pump can deliver pressures up to 60 kPa and can reach output flows up to 40 ml/min. Methane (CH_4) combustion is used as the actuation source. It is worth noting that there are currently no force induced for self-inflating a soft pump and its incorporation in soft robotics. The proposed self-inflating device overcomes this deficiency. The proposed pump system can be used to control the stiffness of the structure

Manuscript received March 16, 2022; final manuscript received June 28, 2022; published online July 19, 2022. Assoc. Editor: Shaoxing Qu.

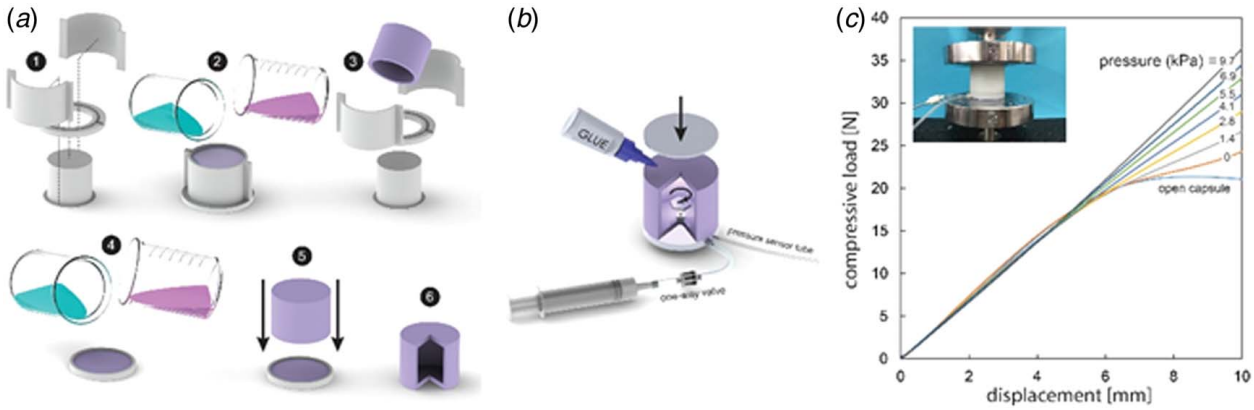

Fig. 1 (*a*) Schematic of multi-step molding procedure used for fabrication of a fully enclosed cylinder made out of curable silicon rubber. This mold is made of four different 3D printed components and enable the easy release of the cured silicon rubber from the mold, (*b*) A syringe is connected to the silicon rubber cylinder through a one-way valve to adjust and maintain the internal air pressure of the cylinder. In addition, two 3D printed rigid plates are glued to the top and bottom faces of the cylinder to prevent bulging and collapsing of the cylinder during the inflation, and (c) A compression test was performed on a pressurized cylinder with internal air pressure values ranging from 0 to 9.7 (kPa). Each testing sample was compressed for 10 mm and plots show the effect of the initial internal air pressure on the force versus displacement of each sample.

with many applications in soft robotics which relies only to external loading applied to the device.

In this paper, we propose a novel structural solution for the development of a self-inflating mechanical structure with flexible embedded fluid pump. The proposed structure operates independent of any external pressurized fluid source and offers a fully flexible self-inflating structure with easy integration with other soft systems.

The proposed structure inhales and stores the ambient air internally when it experiences an external compressive load. The residual internal pressure increases as a function of the intensity of applied compressive loads and the initial internal air pressure inside the system. Repeating this loading cycle results in a gradual increase in the internal air pressure until it reaches a steady-state pressure equilibrium after several loading cycles. This family of self-inflating structures can be widely used in medical devices and automotive industries because of their high reliability and low fabrication cost stemming from their simple working principle and design. This self-inflating mechanical structure comprises of two internal air chambers connected through multiple air channels, see Fig. 2(*a*). The first chamber is located at the top of the structure resembling a dome construct and acts as the embedded flexible fluid pump (shown as pump). The second chamber is attached to the bottom of the pump chamber and stores the pressurized air (shown as capsule).

1.1 Fabrication and Characterization of Inflatable Capsule. We first study the baseline compressive performance of pressurized elastomeric capsule. We will subsequently compare the results to those from the self-inflating structure (integrated pump and capsule) to validate the performance and effectiveness of the proposed self-inflating system.

A closed cylindrical capsule with radius of 60 mm, height of 60 mm, and wall thickness of 5 mm is fabricated through multi-step molding of silicone rubber as shown in Fig. 1(*a*). The top face and the sidewall are molded together using a multi-component separable 3D printed mold (please see Section 3). Silicone rubbers are curable elastomers with excellent properties such as thermal stability and enhanced elongation [25], which make them a promising candidate for inflatable systems experiencing large deformation. Two rigid 3D printed plates (please see Section 3) were glued to the top and bottom of the molded rubber capsule to avoid bulging of the top and bottom faces during the inflation. The bottom rigid plate has two embedded air channels, which connect the capsule to a pressure sensor to monitor the air pressure and a syringe to adjust the internal air pressure. A one-way valve was placed at the outlet of the syringe to prevent the backflow and maintain the desired air pressure in the capsule. A sectioned schematic view of the rubbery construct is shown in Fig. 1(*b*).

Compressive testing was subsequently carried out on manufactured capsule by axially compressing the silicon rubber capsule with different initial (before compression) air pressure values using a single-column Instron universal testing machine. In addition, an open capsule configuration was tested where the syringe and the one-way valve were detached from the system (constant atmospheric pressure inside the capsule). In this testing, the cylindrical capsule was axially compressed for 10 mm and the axial load was measured during compression. Figure 1(*c*) shows compressive force versus capsule axial deformation. All the eight tested samples showed an initial linear relation between load and axial deformation (approx. 5 mm displacement). In this region, all sample responses were almost identical and independent of the internal pressure. However, their behavior in the nonlinear region diverged. In this region, the stiffness of the structure dropped depending on the initial internal air pressure. The lowest softening was observed for a capsule with the maximum pressure of 9.7 kPa. The softening was more pronounced for lower initial pressures. The open capsule configuration showed the most pronounced softening (negative slope of the force versus displacement curve) in the second half of the compression test (see Fig. 1(*c*)). We are now in a position to understand the effect of addition of a pump to the capsule.

1.2 Inflation of the Integrated Pump and Capsule—Numerical Simulation. Here, the external syringe is replaced with an embedded pump component, which can pump the pressurized air into the capsule as the structure is subjected to an axial compression. As shown in Fig. 2(*a*), a dome-shaped chamber, henceforth referred to as pump, is attached to the capsule which would collapse under the loading, resulting in pumping of the inside trapped air in the dome into the capsule through the one-way valve #1. After unloading the structure, one-way valve #1 maintains the air pressure inside the capsule and one-way valve #2 brings fresh air into the pump. In addition, the air channel #3 is incorporated in the design for depressurizing as well as measurement of capsule internal pressure. To have a running airflow from the pump to the capsule, the air pressure inside the pump (P_{Pump}) should reach a higher pressure compared to the air pressure inside the capsule. A fluid structure interaction simulation is conducted on the dome-shaped component using ABAQUS (a commercial finite element analysis (FEA) software,

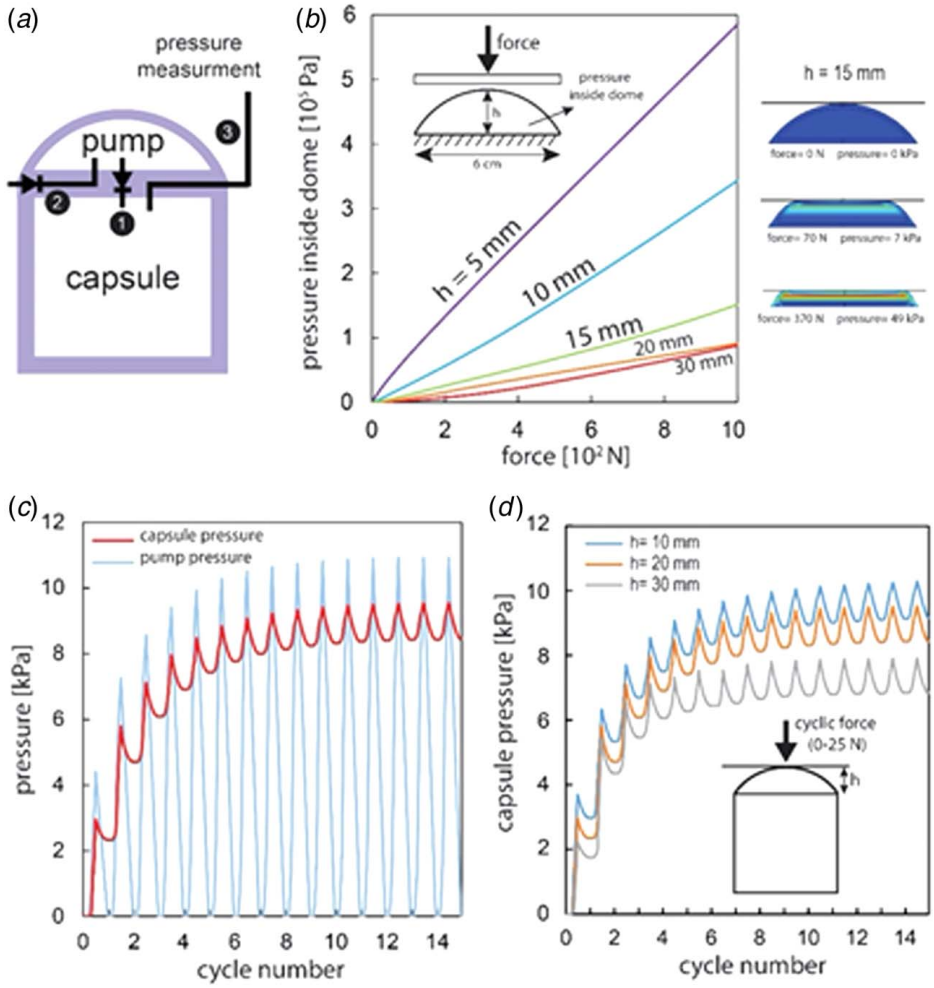

Fig. 2 (*a*) A dome-shaped construct (pump) is attached to the top face of the silicon rubber cylinder (capsule) creating a secondary enclosed volume. The ambient air, pump, and capsule can exchange air through air channels 1–3. Applying compression on the integrated pump and capsule sends the pressurized air from pump to the capsule through channels 1 and pump re-inflates through channel 2 upon load removal. Two shown one-way valves prevent backflow in both channels. In addition, channel 3 is connected to a pressure sensor to measure the internal air pressure of the capsule, (*b*) A finite element model is used to study the effect of dome geometry in compression-induced dome pressure increase. Plots show the internal air pressure versus applied compressive load on the domes with $h = 5$, 10, 15, 20, and 30 mm, (c) A finite element model has been developed in ABAQUS to study the performance of the integrated pump and capsule as a stand-alone system. Plots show the internal air pressure in both pump and capsule during a cyclic compression test, where the force fluctuates between 0 (N) and 25 (N), and (*d*) The same finite element model is used to study the effect of dome geometry in inflation of the structure. Smaller value of dome height results in larger residual pressure after 15 cycles of 25 (N).

Dassault System, France) to further investigate the pressure generation inside the deformable pump. The details of FEAs can be found in Ref. [26]. Fluid structure interaction models the interaction of some movable or deformable structure with an internal or surrounding fluid flow [27]. Figure 2(*b*) shows the numerical result of fluid structure interaction, where the pump pressure versus the axial compressive load applied on dome-shaped component (not including the capsule) is plotted. Considering the geometry of the spherical dome as a portion of a sphere cutoff by a plane, it can be fully quantified using the diameter of the base circle, which is equal to the outer diameter of the capsule (60 mm in this case) and the height of the dome (h). The fluid structure interaction for five different geometries of the air-filled spherical dome with $h = 5$ mm, 10 mm, 15 mm, 20 mm, and 30 mm were numerically simulated, and the results are plotted in Fig. 2(*b*). The results show that shallower domes generate higher pressure for the same value of compressive force compared to a deeper dome. However, shallower domes can pump less amount of air into the capsule in each loading cycle. Hence, based on the desired inflation time and the magnitude of the anticipated external load, an optimal height of the dome can be chosen. The sub-figures of Fig. 2(*b*) show deformation of an air-filled spherical dome with $h = 15$ mm at three different levels of the compression. Next, the cylindrical capsule is also added to the numerical model and a fluid exchange node has been defined between the pump and capsule to account for the air transfer through the one-way valve #1. A minimum requirement of 2 kPa pressure difference is considered for initiating the flow between pump and capsule to count for the opening pressure of the valve. The integrated pump and capsule model with capsule height of 60 mm, capsule outer diameter of 60 mm, capsule wall thickness of 5 mm, dome height of 30 mm, and dome wall thickness of 2 mm was subjected to a cyclic compression loading. In addition,

two rigid circular plates have been added to the model on the top and bottom of the capsule to avoid bulging. Figure 2(*c*) shows the air pressure value inside the pump and the capsule for 15 consecutive compression cycles, where the force fluctuates between 0 N and 25 N. The simulation results show the air pressure in both capsule and pump increases from zero in the first loading cycle. Upon unloading, the pump pressure drops back to zero (fills with fresh air coming through one-way valve #2), while the capsule pressure reduces to a non-zero value as a result of transferring air from the pump to the capsule during the loading. The residual pressure of the capsule (remaining pressure after unloading) gradually increases during the next cycles and eventually reaches a plateau when

$$P_{\text{capsule}} + 2\,\text{kPa} \geq P_{\text{Pump}} \tag{1}$$

where 2 kPa offset between the peak values of P_{capsule} and P_{Pump} accounts for the opening pressure of the one-way valve #1. Figure 2(*d*) shows the effect of dome height (h) on the inflation of the capsule-dome assembly with the previously described geometrical dimensions and loading characteristics. Three different values of 10 mm, 20 mm, and 30 mm have been used as the height of the dome, which corresponds to three plots shown in Fig. 2(*d*). Smaller values of the h result in higher residual air pressure in capsule, however, it requires a greater number of cycles to reach the steady pressure.

1.3 Inflation of the Integrated Pump and Capsule—Experimental. Experimental study is carried on the integrated capsule-dome system to evaluate evolution of capsule internal pressure when the dome is subjected to cyclic axial compression and verify our numerical results. For this, a sample of the proposed self-inflating structure was fabricated. Both capsule and pump were fabricated separately using a multi-step molding technique discussed in Section 3. These two components were glued to each other with a rigid 3D printed plate in between. The plate contains embedded air channels to transfer air between the pump, capsule, ambient environment, and pressure sensor, while passing them through one-way valves to avoid backflow. Please see Fig. 2(*a*) for schematic of the internal air channels and one-way valves. Figure 3(*a*) shows the experimental results of the capsule internal pressure with increase of cyclic compression of the fabricated sample. In this testing, the structure is subjected to 15 consecutive cycles of compressive loading when the force fluctuates between 0 and 25 N. The residual capsule pressure is initially zero and increases gradually until reaching a constant pressure of 10.5 kPa after 13 cycles. The presented results validate the self-inflating functionality of the fabricated sample and shows an excellent agreement with the numerical result presented in Fig. 2. Figure 3(*a*) shows the inflatable structure prior to loading, after four cycles, and after 15 cycles. In Fig. 3(*b*), the stiffening effect is quantified through measurement of the force versus axial displacement of the fabricated sample under the cyclic compression. Each curve in this plot corresponds to a compression cycle. The compressive force is initially related linearly to the displacement, and then it follows by a sudden drop in the stiffness (slope of the curve). The observed drop happens because of valve opening when the trapped air inside the pump opens its way to the capsule chamber. As the number of cycle increases (higher residual pressure in the capsule), the effect of valve opening diminishes and eventually an almost linear force versus displacement curve can be observed after 10 cycles. In general, the overall stiffness of the device after valve opening increases because of structural inflation. Note, the same quality of the stiffening effect captured in the capsule inflation test, presented in Fig. 1(*c*), is also observed in the self-inflating structure. This similarity verifies the performance of the embedded deformable pump as an alternative low-cost method for the external air pump.

1.4 Self-Inflating Tire. The proposed self-inflating structure can be used in various applications, where the on-demand inflation or stiffening of a mechanical construct is desired. An important application of such a device is a self-inflating tire, where the rotation of the tire results in a cyclic loading and provides the energy source for the inflation. In this application, the tire inflation continues until it reaches the desired pressure. The desired pressure can be tuned using an adjustable pressure regulator and the internal tire pressure can be changed based on the road quality, temperature, or driving style [28,29]. Figure 4(*a*) shows schematic of the sectioned self-inflating tire. The structure of the tire is made by revolving the shown cross section, similar to the cross section of the self-inflating structure studied earlier in this paper; see Fig. 2(*a*). In addition, four walls radially divide the internal structure of the tire to four equal sections (walls are placed every 90 deg). The internal structure of the tire includes the pump and the capsule components interacting through a pneumatic unit. The pneumatic unit is located in the rim of the wheel for easier access and fabrication. The applied cyclic loading on the tire causes the pressure increase in the pump component and eventually pumps the pressurized air to the capsule. As discussed in Fig. 3, the capsule pressure increases gradually until it reaches a plateau. Figure 4(*b*) shows two images of a

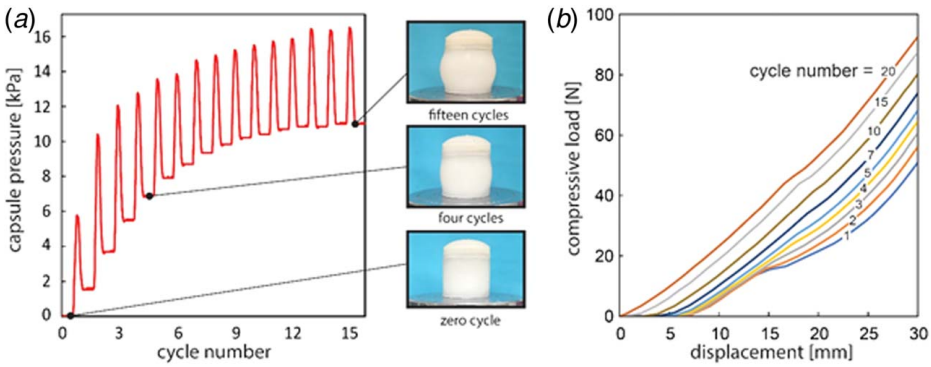

Fig. 3 (*a*) The integrated pump and capsule has been fabricated using a multiple-step silicon rubber molding technique and glued together to form a self-inflating structure. A cyclic compressive load, oscillating between 0 and 25 N, is applied on the structure using an Instron machine and the capsule air pressure versus cycle number is plotted. The residual pressure value of air pressure remains in the capsule after unloading, starts from zero, gradually increases, and eventually plateaus at 10.5 kPa after 13 cycles. The front view of the self-inflating system is shown after zero, four, and 15 cycles, and (*b*) The compressive load versus displacement response of the self-inflating structure is measured experimentally using an Instron machine and plotted for nine non-sequential cycles.

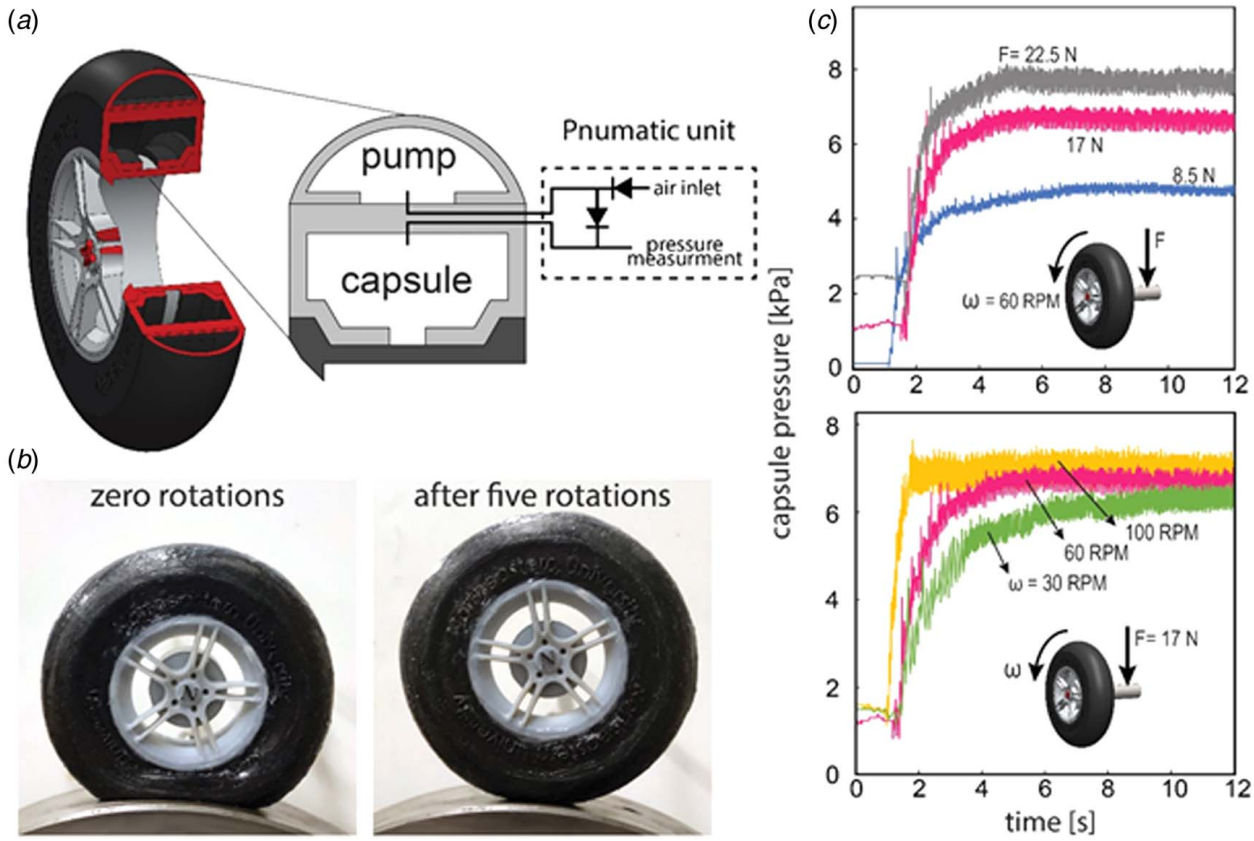

Fig. 4 **(*a*) A self-inflating tire is designed based on the previously studied self-inflating cylindrical structure. The tire is created by revolving the shown cross section around the wheel axis. The cross section consists of a capsule and a dome-shaped pump (similar to the self-inflating cylinder design). Two internal channels connect the pump and capsule to an external pneumatic unit, which carry out the flow transfer and pressure measurement, (*b*) The self-inflating tire is fabricated using a PloyJet 3D printing technique. The pump and capsule were printed separately out of TangoBlackPlus (Stratasys Inc.), the rim is printed out of VeroWhite (Stratasys Inc.), and all are glued together. The low-pressure and high-pressure states of the tire have been shown after zero and five rotations, respectively, while a downward force of 17 N is applied on the wheel axis, and (*c*) The internal pressure of tire (air pressure in capsule) is plotted for two scenarios: (1) wheel rotates with a constant speed of 60 rpm and three different loads of 8.5, 17, and 22.5 N are applied vertically on the wheel axle. (2) A constant vertical load of 17 N is applied on the wheel axle and the wheel rotates with three different speeds of 30, 60, and 100 rpm.**

fabricated self-inflating tire prior to loading (depressurized) and after five full rotations (pressurized). See Section 3 for more information on the fabrication of the self-inflating tire. To validate the expected performance of the fabricated self-inflating tire, an experimental testing is performed. In this testing, a vertical downward load is applied on the wheel axle and the wheel is located on a moving surface with adjustable speed. In the first part of the testing, three different force values of 8.5 N, 17 N, and 22.5 N are applied on the wheel axle, while the wheel is rotating at 60 rpm. Figure 4(*c*) shows that the tire pressure increases as a function of time. The initial tire air pressure depends on the axial force and as the tire rotates, the pressure gradually increases until it reaches a plateau. The final tire pressure is higher for greater axial load. In the second part of the testing, the rotational speed of tire has been set to three different values of 30 rpm, 60 rpm, and 100 rpm while the axial load is maintained constant at 17 N for all three cases. Figure 4(*c*) bottom shows the capsule pressure as a function of time, where the higher rotational speed causes a faster pressure increase in the tire and the final steady-state pressure is almost independent of the rotational speed.

2 Materials and Methods

Self-inflating cylinder: This structure is made through multi-step molding of Dragon Skin FX-Pro (Smooth-On Inc., Macungie, PA). Dragon Skin FX-Pro is a soft and durable platinum silicone rubber with a core hardness of 2 A and break elongation of 763%, which makes it a proper choice for deformable structures. Dragon skin FX-Pro comes in two different containers of A and B which should be mixed with a ratio of 1:1 (volume or weight), poured to the mold and left to dry for at least 40 min in room temperature. All molds are 3D printed using VeroWhite material in an Eden 260 V Polyjet 3D printer (Stratasys Ltd.). As shown in Fig. 1(*a*), the cylinder is made of two separate components: (1) sidewall and top face, which is made using a three-piece mold to ease the mold release process, and (2) bottom face, which is made using a one-piece mold. These two components were later glued together using Sil-Poxy (Smooth-On Inc., Macungie, PA) to form a fully enclosed construct. In addition, the internal channels are 3D printed and attached to the cylinder. The structure shown in Figs. 2 and 3 includes an additional dome-shaped top layer, which is molded separately and glued to the cylinder top face to form the final self-inflating structure.

2.1 Self-Inflating Tire. This construct includes a rigid rim with embedded air channels to enable air transfer between the ambient air and tire. The rim is 3D printed using VeroWhite material in an Eden 260 V Polyjet 3D printer (Stratasys Ltd.). Tire, including embedded air channels, is 3D printed in two separate parts using TangoBlackPlus material in the same 3D printer. TangoBlackPlus offers properties similar to rubber (tensile strength of 0.8–2.4 MPa and 170–220% elongation at break). Two 3D

printed components of the tire are glued together and later glued to the rim using Sil-Poxy (Smooth-On Inc., Macungie, PA) to create a sealed connection. Finally, eight one-way air valves are assembled externally to the rim to control the airflow direction as described in the paper.

Pressure measurement: A Honeywell HSCDRRN005PD2A5 pressure sensor was used to measure the internal air pressure of the self-inflating cylinder and tire. An Arduino Uno is used as the controller board to process and save the pressure sensor data.

3 Conclusions

Inflatable structures are commonly used in a variety of engineering applications such as robotics, space structures, medical devices, and automotive safety devices. A novel design for a self-inflating structure with an embedded soft fluid pump is introduced. The performance of this conceptual device is fully characterized and validated by the finite element method and experimentation. It is shown with this design a self-inflating silicon rubber cylinder is capable to increase its internal air pressure from 0 to 10 kPa when the dome is subjected to 15 cyclic compressions of 0–25 N. The self-inflating cylinder design was used as a foundation in the design of new generation of self-inflating structures such as tires, which harvests the applied cyclic loading on the tire, as a result of tire rotation and weight of the vehicle, to pressurize the tire without any external air pump. It is shown again that the tire can be pressurized using this conceptual design. The speed of inflation depends on the tire speed and the compressive load to the axel of the tire.

Acknowledgment

This work was partially supported by the National Science Foundation and Department of Mechanical and Industrial Engineering of Northeastern University.

Conflict of Interest

There are no conflicts of interest.

Data Availability Statement

The authors attest that all data for this study are included in the paper.

References

[1] Freeland, R., Bilyeu, G., Veal, G., and Mikulas, M., 1998, "Inflatable Deployable Space Structures Technology Summary," 49th International Astronautical Congress, Melbourne, Australia, Sept. 28–Oct. 2, pp. 1–16.
[2] Kiper, G., and Soylemez, E., 2009, "Deployable Space Structures," 2009 4th International Conference on Recent Advances in Space Technologies, Istanbul, Turkey, June 11–13, IEEE, pp. 131–138.
[3] Schenk, M., Viquerat, A. D., Seffen, K. A., and Guest, S. D., 2014, "Review of Inflatable Booms for Deployable Space Structures: Packing and Rigidization," J. Spacecr. Rockets, **51**(3), pp. 762–778.
[4] Mutlu, R., Alici, G., and Li, W., 2012, "Kinematic Analysis of Electroactive Polymer Actuators as Soft and Smart Structures With More DoF Than Inputs," IEEE/ASME International Conference on Advanced Intelligent Mechatronics (AIM), Kaohsiung, Taiwan, July 11–14, IEEE, pp. 484–489.
[5] Ahn, S.-H., Lee, K.-T., Kim, H.-J., Wu, R., Kim, J.-S., and Song, S.-H., 2012, "Smart Soft Composite: An Integrated 3D Soft Morphing Structure Using Bend-Twist Coupling of Anisotropic Materials," Int. J. Precis. Eng. Manuf., **13**(4), pp. 631–634.
[6] Gao, W., and Ramani, K., 2012, "Kaleidogami™: Multi-Primitive Reconfigurable Artistic Structures," Hyperseeing, Special Issue on Shape Modeling International, Fabrication and Sculpting Event & Exhibition, College Station, TX, May 22–25, pp. 27–34.
[7] Séquin, C. H., 2016, "Reconfigurable Snap-Together Sculpting," Comput. Aided Des. Appl., **13**(1), pp. 1–13.
[8] Kamrava, S., Ghosh, R., Wang, Z., and Vaziri, A., 2019, "Origami-Inspired Cellular Metamaterial With Anisotropic Multi-Stability," Adv. Eng. Mater., **21**(2), p. 1800895.
[9] Kamrava, S., Mousanezhad, D., Ebrahimi, H., Ghosh, R., and Vaziri, A., 2017, "Origami-Based Cellular Metamaterial With Auxetic, Bistable, and Self-Locking Properties," Sci. Rep., **7**(1), pp. 1–9.
[10] Xie, Z., Domel, A. G., An, N., Green, C., Gong, Z., Wang, T., Knubben, E. M., et al., 2020, "Octopus Arm-Inspired Tapered Soft Actuators With Suckers for Improved Grasping," Soft Robot., **7**(5), pp. 639–648.
[11] Yang, D., Mosadegh, B., Ainla, A., Lee, B., Khashai, F., Suo, Z., Bertoldi, K., and Whitesides, G. M., 2015, "Buckling of Elastomeric Beams Enables Actuation of Soft Machines," Adv. Mater., **27**(41), pp. 6323–6327.
[12] Adams, W., Sridar, S., Thalman, C. M., Copenhaver, B., Elsaad, H., and Polygerinos, P., 2018, "Water Pipe Robot Utilizing Soft Inflatable Actuators," 2018 IEEE International Conference on Soft Robotics (RoboSoft), Livorno, Italy, Apr. 24–28, IEEE, pp. 321–326.
[13] Lee, C., Kim, M., Kim, Y. J., Hong, N., Ryu, S., Kim, J., and Kim, S., 2017, "Soft Robot Review," Int. J. Control Autom. Syst., **15**(1), pp. 3–15.
[14] Usevitch, N. S., Hammond, Z. M., Schwager, M., Okamura, A. M., Hawkes, E. W., and Follmer, S., 2020, "An Untethered Isoperimetric Soft Robot," Sci. Rob., **5**(40), pp. 1–14.
[15] O'Neill, C., Proietti, T., Nuckols, K., Clarke, M. E., Hohimer, C. J., Cloutier, A., Lin, D. J., and Walsh, C. J., 2020, "Inflatable Soft Wearable Robot for Reducing Therapist Fatigue During Upper Extremity Rehabilitation in Severe Stroke," IEEE Robot. Autom. Lett., **5**(3), pp. 3899–3906.
[16] Park, J., Choi, J., Kim, S. J., Seo, K.-H., and Kim, J., 2020, "Design of an Inflatable Wrinkle Actuator With Fast Inflation/Deflation Responses for Wearable Suits," IEEE Robot. Autom. Lett., **5**(3), pp. 3799–3805.
[17] Rafsanjani, A., Zhang, Y., Liu, B., Rubinstein, S. M., and Bertoldi, K., 2018, "Kirigami Skins Make a Simple Soft Actuator Crawl," Sci. Robot., **3**(15), p. eaar7555.
[18] Konishi, S., and Kosawa, H., 2020, "High-Output Bending Motion of a Soft Inflatable Microactuator With an Actuation Conversion Mechanism," Sci. Rep., **10**(1), pp. 1–10.
[19] Gorissen, B., Melancon, D., Vasios, N., Torbati, M., and Bertoldi, K., 2020, "Inflatable Soft Jumper Inspired by Shell Snapping," Sci. Rob., **5**(42), pp. 1–7.
[20] Cacucciolo, V., Shintake, J., Kuwajima, Y., Maeda, S., Floreano, D., and Shea, H., 2019, "Stretchable Pumps for Soft Machines," Nature, **572**(7770), pp. 516–527.
[21] Sinn, T., Vasile, M., and Tibert, G., 2012, "Design and Development of Deployable Self-Inflating Adaptive Membrane," 53rd AIAA/ASME/ASCE/AHS/ASC Structures, Structural Dynamics and Materials Conference 20th AI, Apr. 23–26, Honolulu, HI, AIAA 2012-1517.
[22] Diteesawat, R. S., Helps, T., Taghavi, M., and Rossiter, J., 2021, "Electro-Pneumatic Pumps for Soft Robotics," Sci. Robot., **6**(51), p. eabc3721, pp. 1–11.
[23] Yamaguchi, T., Yamamoto, D., Arie, T., Akitaa, S., and Takei, K., 2020, "Wrist Flexible Heart Pulse Sensor Integrated With a Soft Pump and a Pneumatic Balloon Membrane," RSC Adv., **10**(29), pp. 17353–17358.
[24] Stergiopulos, C., Vogt, D., Tolley, M. T., Wehner, M., Barber, J., Whitesides, G. M., and Wood, R. J., 2014, "A Soft Combustion-Driven Pump for Soft Robots," Proceedings of the ASME 2014 Conference on Smart Materials, Adaptive Structures and Intelligent Systems SMASIS2014, Sept. 8–10, Newport, RI, SMASIS2014-7536.
[25] Polmanteer, K. E., 1988, "Silicone Rubber, Its Development and Technological Progress," Rubber Chem. Technol., **61**(3), pp. 470–502.
[26] Kamrava, S., 2020, "Mechanics of Origami Structures," Ph.D. thesis, Department of Mechanical Engineering, Northeastern University, Boston, MA.
[27] Bungartz, H.-J., and Schäfer, M., 2007, *Fluid-Structure Interaction: Modelling, Simulation, Optimisation*, Springer Science & Business Media, Berlin/Heidelberg.
[28] Ferguson, S. C., 1998, "Variable Tire Pressure Traction Control Enhancement," Google Patents.
[29] Owende, P. M., Hartman, A. M., Ward, S. M., Gilchrist, M. D., and O'Mahony, M. J., 2001, "Minimizing Distress on Flexible Pavements Using Variable Tire Pressure," J. Trans. Eng., **127**(3), pp. 254–262.